Available online at www.sciencedirect.com

ScienceDirect

Additive Manufacturing 1–4 (2014) 119–126

Additive MANUFACTURING

www.elsevier.com/locate/addma

Integrated control of solidification microstructure and melt pool dimensions in electron beam wire feed additive manufacturing of Ti-6Al-4V☆

Joy Gockel[a,*], Jack Beuth[a], Karen Taminger[b]

[a] *Department of Mechanical Engineering, Carnegie Mellon University, 5000 Forbes Avenue, Pittsburgh, PA 15213, United States*
[b] *NASA Langley Research Center, MS 188A, Hampton, VA 23681, United States*

Available online 7 October 2014

Abstract

The ability to deposit a consistent and predictable solidification microstructure can greatly accelerate additive manufacturing (AM) process qualification. Process mapping is an approach that represents process outcomes in terms of process variables. In this work, a solidification microstructure process map was developed using finite element analysis for deposition of single beads of Ti-6Al-4V *via* electron beam wire feed AM processes. Process variable combinations yielding constant beta grain size and morphology were identified. Comparison with a previously developed process map for melt pool geometry shows that maintaining a constant melt pool cross sectional area will also yield a constant grain size. Additionally, the grain morphology boundaries are similar to curves of constant melt pool aspect ratio. Experimental results support the numerical predictions and identify a proportional size scaling between beta grain widths and melt pool widths. Results further demonstrate that *in situ* indirect control of solidification microstructure is possible through direct melt pool dimension control.

1. Introduction

Direct metal additive manufacturing (AM) processes are attractive for aerospace and other industries producing complex, high cost components [1]. For small batch part production, AM incurs minimal initial cost when compared to traditional manufacturing processes such as casting or forging. AM can also be used in combination with traditional processes to decrease fabrication costs for large components with detailed features. For example, machining of large, forged components incurs large costs, and creates significant amounts of material waste. In contrast, a simple forging can be manufactured with detailed features created by adding material *via* AM, saving both material and cost. Additive manufacturing can also be used for repair of cracks or worn components [2].

While AM offers the promise of increased efficiency and flexibility compared to conventional manufacturing, widespread commercialization of AM processes requires the ability to predict and control melt pool dimensions, solidification microstructure, residual stress and other process outcomes in terms of process variables. Melt pool dimension control is needed to accurately build a geometry and melt pool dimensions determine process precision. Microstructure control is needed to produce reliable and repeatable mechanical properties. Residual stress control is needed to maintain part geometry until stress-relieving post processing can take place. Various forms of process mapping approaches have been developed for control of melt pool dimensions and residual stress through a wide range of processing variables [3–6]. However, the ability to correctly deposit a part is not sufficient if the microstructure and resulting mechanical properties of the completed part are not suitable for the desired application [7].

Many different materials can be used in direct metal AM processes. Ti-6Al-4V (Ti64) is used in the aerospace industry due

☆ One or more authors of this article are part of the Editorial Board of the journal. Full responsibility for the editorial and peer-review process for this article lies with the journal's Editor-in-Chief Prof. Ryan Wicker and Deputy Editor Prof. Eric MacDonald. Furthermore, the authors of this article had no and do not currently have access to any confidential information related to its peer-review process.

* Corresponding author. Tel.: +1 412 268 3873; fax: +1 412 268 3348.
E-mail addresses: joy.gockel@gmail.com (J. Gockel), beuth@andrew.cmu.edu (J. Beuth).

http://dx.doi.org/10.1016/j.addma.2014.09.004
2214-8604/

to its light weight, corrosion resistance, and high strength properties even at high temperatures [8]. The mechanical properties of Ti64 are dependent on the solidification microstructure (grain size and morphology) [9,10], which is controlled by the thermal conditions at the onset of solidification [11]. More specifically, Ti64 is a two-phase, alpha-beta titanium alloy. The cooling rate at the liquidus temperature (1893 K) determines the beta grain size and cooling rate and thermal gradient determine grain morphology. The alpha grain size can be determined by cooling rates at the beta transus temperature (1270 K) and below [10] Many material properties are governed by the alpha grain size, but they are typically modified by post process heat treatment. It has been suggested that the beta grain structure is the dominating factor for other mechanical properties, such as fatigue behavior. More importantly, the beta grain structure typically remains unchanged through traditional heat treatments [9,10]. Therefore, for AM applications it is crucial to obtain suitable, as-deposited beta grain size and morphology. In this work, the term solidification microstructure refers to the beta grain size and morphology.

2. Background

In many applications, in order to replace traditional manufacturing with additive manufacturing, comparable to or better than wrought mechanical properties must be obtained. The mechanical properties of a variety of geometries built using different types of AM processes have been explored. Results show that materials produced by additive manufacturing can have mechanical properties [12,13] and fatigue limits [14,15] comparable to wrought materials. However, a change in processing conditions may produce a change in the resulting properties [3].

Characterization of the microstructure of a material can be used to draw conclusions about the resulting mechanical properties [9,10]. Many in the material science and manufacturing communities have explored the effect of processing on solidification microstructure produced by additive manufacturing [16–19]. Though significant insights have been gained through post process experimental characterizations, the results are limited to specific cases. Currently, identifying microstructural trends through post process characterization of material requires much iteration, both in academic and industrial studies.

Ultimately, microstructure must be determined in terms of process variables in order to control microstructure while also controlling melt pool geometry, residual stress, flaw formation and other process outcomes. To this end, Bontha et al. developed a particular version of thermal process maps for predicting trends in solidification microstructure in terms of process variables [20–22]. Kobryn et al. investigated the role of process variables on microstructure and mechanical properties through experimentation and observation of solidification behavior [11,23]. These foundational studies predict the microstructure in terms of individual process variables, which limits their usability in process control applications.

In this work, a patent-pending process mapping approach [24] applicable to the building of 3-D shapes across multiple direct metal AM processes was used to represent solidification microstructure predictions in terms of two primary process variables (beam power, P, and beam travel velocity, V). An extension of previous work by the authors [25], the process map for solidification microstructure was created for single bead deposits by an electron beam wire feed AM process (*e.g.* the Electron Beam Freeform Fabrication (EBF3) process developed at NASA Langley or the commercially developed Direct Manufacturing process by Sciaky). The EBF3 process melts wire being feed into the system, similar to a welding process, rather than selectively melting a bed of power like in other additive manufacturing processes. Solidification microstructure was predicted using the solidification map for Ti64 [11] and the cooling rates and thermal gradients from thermal finite element models. The solidification data was used to plot curves of constant cooling rate and the grain morphology boundaries in beam power *versus* travel velocity (P–V) space, creating a P–V process map for microstructure control.

Solidification microstructure predictions were then related to an analogous P–V process map for controlling melt pool dimensions [26]. This allows exploration of the ability for indirect *in situ* microstructure control through melt pool dimension control. Single bead deposit experimental observations are presented and related to the predictions. The study of microstructural features of Ti64 and their relationship to mechanical properties is complicated. This paper is limited to the consideration of solidification microstructure (beta grain size and morphology). However, an important contribution of this work is that the solidification microstructure process map presented herein can guide additional experimental and modeling studies of microstructure for AM processes by identifying beam power and travel speed combinations of interest.

3. Modeling methods

3.1. Process mapping

Process mapping is an approach that maps process characteristics as a function of primary process variables based on simulation or experimental results [6,24]. This approach allows for understanding and expansion of AM processing space. Beam power (P) and beam travel velocity (V) have been identified as two primary process variables. Other primary process variables are material feed rate (MFR or other variable defining MFR), existing temperature of the component being deposited onto (T_0) and feature geometry (the local geometry of the part, which can be represented by one or more geometric variables). While it is recognized that, depending on the process, other process variables (such as average powder particle size or beam spot size) may affect process outcomes, the approach involves mapping AM processes in terms of the five primary process variables first. Once that behavior is mapped, if needed, a detailed study of the role of a secondary process variable can be carried out to evaluate its effects on the process across the full five-primary-variable processing space. In this work, the process characteristics of interest were the beta grain size and morphology determined at solidification.

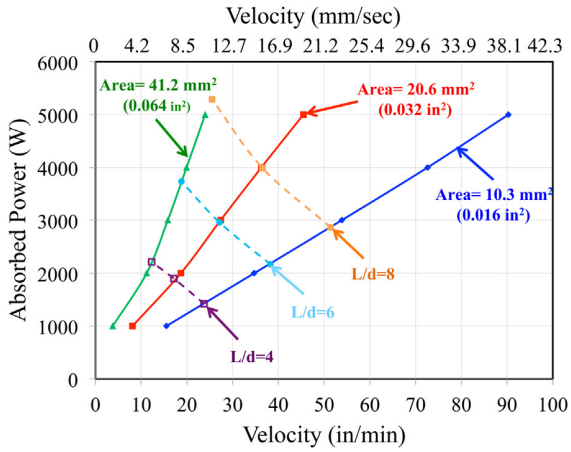

Fig. 1. Process map for controlling melt pool dimensions for single bead deposits of Ti64.

Fig. 1 shows an updated version of a previously developed *P–V* process map for melt pool dimension control for electron beam wire feed AM processes. This map is for the geometry of a single bead deposited in the middle of a large part, with $T_0 = 373$ K and a ratio of added material to total material being melted of $\phi = 0.77$. Compared to the process map given by Soylemez [26], melt pool area values have been adjusted slightly and additional simulations have been run to more accurately determine locations of the plotted curves. Curves of constant melt pool cross sectional area, *A* (a melt pool size metric), as well as curves of constant melt pool length to depth ratio, *L/d* (a melt pool shape metric), were plotted [26,27]. As indicated in Fig. 2, melt pool cross sectional area is the largest melt pool area perpendicular to the travel velocity direction (defined as the *x* direction in this paper). Melt pool length is the *x* distance between the location of maximum melt pool cross sectional area and the trailing end of the melt pool. The depth is an effective depth, which was determined from the cross sectional area making the assumption that the area is a semi-circle (the actual depth could also be used, but use of an effective depth yields a direct link to melt pool cross sectional area). By following curves of constant *A* or *L/d*, this *P–V* process map for melt pool dimension control allows these quantities to be maintained across *P* and *V* values differing by as much as a factor of 5.

3.2. Material added finite element models

Thermal finite element simulations in ABAQUS were used to model single bead deposition and the addition of material by the wire feeder. The thermal gradient and cooling rate were obtained as the temperature changes from the liquid to solid range along the trailing edge of the melt pool as indicated in Fig. 2. Material was added ahead of the heat source at each step at specified time increments to simulate the travel velocity as shown in Fig. 3, and for all simulations in this study a value of $\phi = 0.77$ is used. Because the deposition takes place in a vacuum, the 3-D models do not include convective heat transfer on their vertical and top surfaces. The nodes have an initial temperature of $T_0 = 373$ K and a constant temperature of 373 K specified at the base of the model, which is similar to the temperatures in the EBF3 process. Eight-node, linear brick elements were used throughout the model. As shown in Fig. 4, the mesh is biased toward the top surface and was refined in the region where data were extracted, in order to reduce computation time while providing sufficient element density to resolve solidification cooling rates and thermal gradients. Studies were conducted to insure convergence of the thermal gradients and cooling rates extracted from the simulations as a function of element density in and around the melt pool. Element sizes in and around the melt pool were scaled with melt pool size to maintain a sufficient number of elements across all simulations. A distributed heat flux was applied along the top of the added bead to simulate rapid beam oscillation across the melt pool, which is used in the EBF3 process to reduce the concentration of heat on the surface. Temperature-dependent thermal properties and latent heat were included.

3.3. Solidification map for Ti64

Solidification maps are used to predict the solidification microstructure based on the thermal conditions at the onset of solidification. The solidification map for Ti64 is seen in Fig. 5. The *y*-axis is the variable *G*, which is the magnitude of the thermal gradient vector at a location on the solidification boundary. *R* is the solidification rate, which is on the *x*-axis. The solidification rate is defined as $R = (1/G)(\partial T/\partial t)$, where $(\partial T/\partial t)$ is

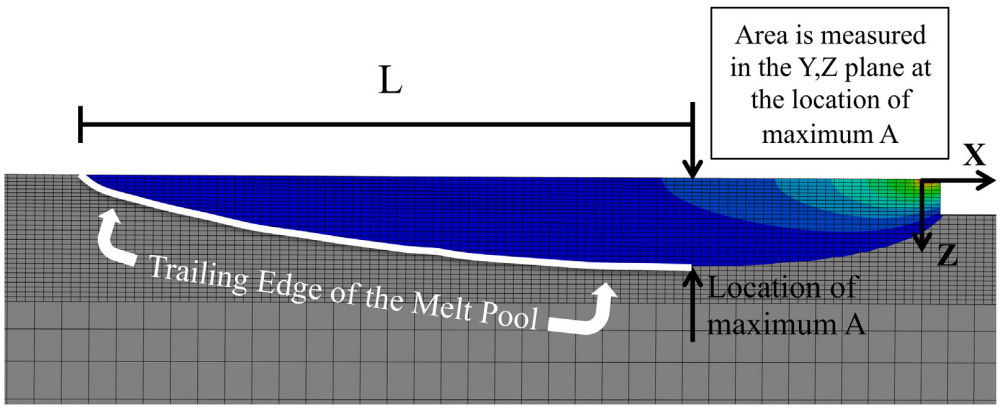

Fig. 2. Melt pool contour including the solidification front.

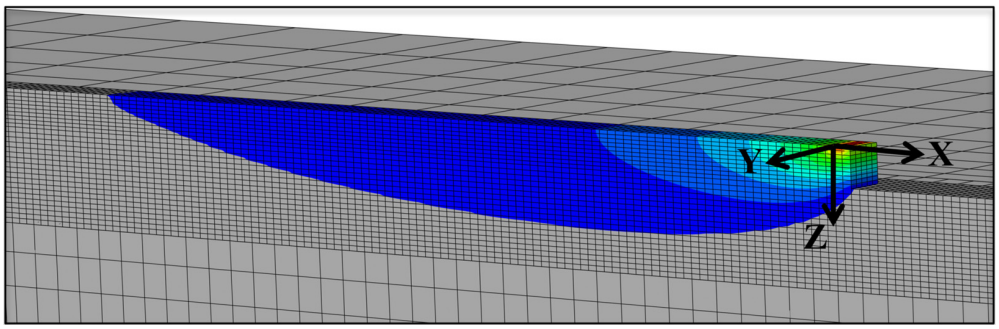

Fig. 3. Material being added to the finite element model.

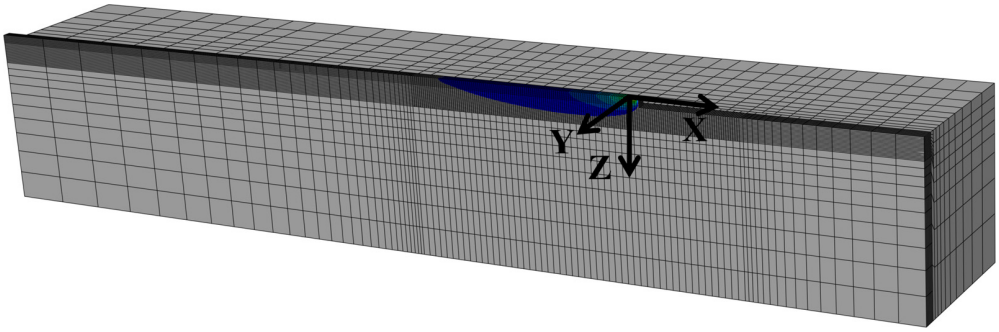

Fig. 4. Finite element mesh.

the cooling rate (derivative of the temperature, T with respect to the time, t) at the onset of solidification at a single location on the solidification boundary. Diagonal lines with negative slope on the solidification map are curves of constant cooling rate at solidification and thus correspond to curves of constant beta grain size. The regions defined on the solidification map correspond to the grain morphology: fully equiaxed, mixed or fully columnar. Columnar grains are elongated in one direction while equiaxed grains have roughly the same dimension in all directions. Grain morphology regions are based on an analytical model developed by Hunt [28] and have been determined for additive manufacturing through experimental calibration by Kobryn et al. [11]. In this research, the thermal conditions used to predict the solidification microstructure are obtained using material added finite element models. This approach follows methods for process mapping of microstructure developed by Klingbeil et al. [20–22].

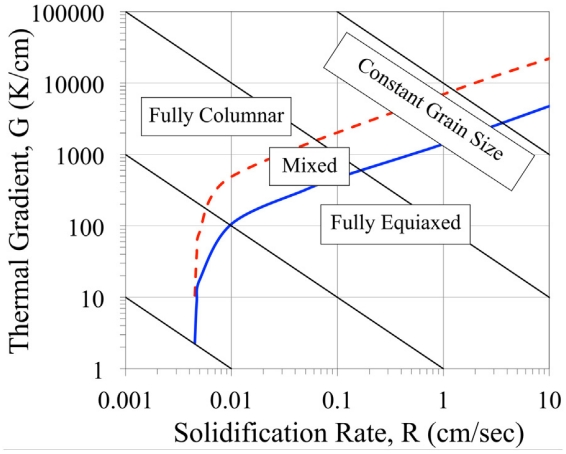

Fig. 5. Solidification map for Ti64.

4. Modeling results

4.1. P–V *process map for microstructure control*

Solidification maps predict microstructure in terms of thermal gradient and solidification rate, but are difficult to use by process operators. Monitoring the cooling rates and thermal gradients *in situ* is difficult and can only be observed on the surface, so it is rarely done. Even in cases where monitoring of cooling rates and thermal gradients is practical, the solidification map only provides results for individual values of G and R, and does not provide a guide to controlling solidification microstructure across process variables. Therefore, A P–V process map for solidification microstructure has been developed in order to identify paths through or regions of processing space with constant grain size and different grain morphologies.

The grain morphology data from the G *versus* R plot in Fig. 5 have been translated onto a plot of beam power *versus* beam velocity and the curves of constant cooling rate have been identified using material added finite element simulations. For one power and velocity combination, the resulting thermal gradients and solidification rates span up to an order of magnitude each along the solidification front. The results presented here are for the top of the melt pool, which is a critical location, where the lowest gradients are present and the transition to a mixed

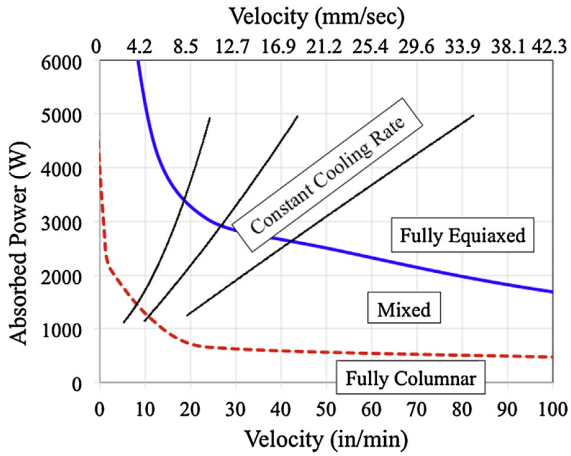

Fig. 6. Process map for controlling solidification microstructure of single bead deposits of Ti64.

or equiaxed grain morphology will first take place. Therefore, power and velocity combinations yielding thermal conditions for fully equiaxed grains at the top of the melt pool will generally still have thermal conditions yielding columnar grains into the melt pool depth, yielding a deposit with a mix of equiaxed and columnar grains.

The resulting *P–V* process map for controlling solidification microstructure for single bead deposits of Ti64 in an electron beam wire fed process shown in Fig. 6 (for $T_0 = 373$ K and $\phi = 0.77$). The curves of constant cooling rate in *P–V* space were identified by the solid black curves. These curves are almost linear in this region of *P–V* space. It is possible to maintain a constant beta grain size while moving from low powers and low velocities, to high powers and high velocities (and higher deposition rates) if the identified path is followed. The dashed line represents the boundary between fully columnar and mixed grain morphology. The boundary between mixed and fully equiaxed grain morphology is the curved solid line. These curves define the boundaries of three regions where columnar, mixed and equiaxed grain morphologies exist at the top of the melt pool. As a rule of thumb, the transition from fully columnar to columnar plus equiaxed grains occurs as *P* and *V* are both increased. The solidification microstructure process map can be used when planning deposition parameters to balance high deposition rates with specific grain size and morphology constraints. It should be noted that a *P–V* map analogous to that of Fig. 6 was presented in the conference paper of reference [25]. The current plot shows slightly different and more accurate results, obtained from a larger number of process simulations.

4.2. Integrated control of microstructure and melt pool dimensions

Currently, post processing and microscopy are required to observe AM solidification microstructure. By combining the results of Figs. 1 and 6, solidification microstructure can be directly related to melt pool dimensions. When comparing the process map for solidification microstructure in Fig. 6 to the process map for melt pool dimensions in Fig. 1, connections can be drawn between the two process maps. The curves of constant grain size are similar to the curves of constant melt pool cross sectional area, *A*. In other words, by controlling *A* (which can be related to melt pool width, which is observable in real time during processing), a constant beta grain size is also maintained. The grain morphology region boundaries are similar to curves of constant length-to-depth ratio. The boundary represents the point where the morphology transition will first take place. As a result, an operator can observe the aspect ratio of the melt pool and use that to infer grain morphology.

Melt pool size and shape cannot be independently controlled, with corresponding consequences for microstructure control. While keeping the melt pool area constant and increasing the deposition rate (by increasing *P* and *V*), the grain size will remain constant, but the length to depth ratio will become larger and a transition to some equiaxed grains, and then more equiaxed grains will occur. Integration of the solidification microstructure and melt pool dimension process maps allows the ability to indirectly plan and control solidification microstructure by controlling melt pool size and shape in real time. This type of *in situ* microstructure control allows for the potential to tailor the microstructure and the resulting mechanical properties in specific regions of a part build using direct metal AM, with substantially fewer trial and error type tests.

5. Single bead deposit experiments

Single bead deposit experiments were performed by the NASA Langley Research Center in order to assess model predictions. The NASA EBF^3 system is a modified Sciaky electron beam system with a wire feed. The EBF^3 process uses an electron beam as the power source with a wire feed for depositing material, similar to the welding process. The substrate table moves under the beam at a specified direction and travel velocity to create the shape of the part. The wire feeder then moves up and the next layer is deposited in the same manner. The experiments performed were deposition of a single bead of Ti64 onto a substrate of the same material using various beam powers and velocities spanning a factor of 5 with the same predicted melt pool area [26]. Three different areas were investigated: Blue: 10.3 mm^2 (0.016 in^2), Red: 20.6 mm^2 (0.032 in^2), and Green: 41.2 mm^2 (0.064 in^2). The process variables used are shown in Table 1. In Table 1 the absorbed power is simply 90% of the source power for each case, where an assumed beam absorptivity of 0.90 has yielded very good agreement between predicted and experimentally measured melt pool dimensions for this process [26]. Specimens were sectioned normal to the bead length at two locations along the bead length in the steady-state portion of the bead. These specimens were mounted, mechanically polished using 240–600 grit silicon carbide grit paper, 6 and 1 μ monocrystalline diamond slurry with activated mastermet and etched using Kroll's etchant in order to observe the solidification microstructure using optical microscopy. Beta grain widths were measured using the standard intercept method [29]. The melt pool area was also measured and the effective width was

Table 1
Processing parameters for single pass experiments.

Source power (Watts)	Absorbed power (Watts)	Travel velocity (in/min)	Travel velocity (mm/s)	Wire feed rate (in/min)	Wire feed rate (mm/s)
Blue					
1400	1250	16.1	6.8	63	27
1650	1500	21.5	9.1	85	36
2200	2000	31.9	13.5	125	53
3350	3000	52	22	162	69
4450	4000	68.3	28.9	204	86
5550	5000	85	36	335	142
Red					
1400	1250	5.7	2.4	45	19
1650	1500	8.3	3.5	64	27
2200	2000	13.9	5.9	108	46
2800	2500	19.2	8.1	150	63
3350	3000	23.6	10	184	78
4450	4000	32.8	13.9	256	108
5550	5000	42.5	18	334	141
Green					
1650	1500	2.2	0.9	35	15
2220	2000	5.2	2.2	82	35
3350	3000	10.9	4.6	171	72
5550	5000	19.4	8.2	306	130

calculated with the assumption that the melt pool area is a semi-circle and the effective width is the diameter of the semi-circle.

5.1. Experimental results

Beta grain size and morphology have been assessed using single bead deposit experiments. As indicated in the plot of Fig. 7, clear evidence of equiaxed grains was found in experiments within the predicted fully equiaxed region, with the exception of the experimental cases with the smallest melt pool area. Additional investigation is needed to determine why this was the case. Micrographs moving from low power to high power for the melt pool areas of 10.3 mm^2 (0.016 in^2), 20.6 mm^2 (0.032 in^2), and 41.2 mm^2 (0.064 in^2) are seen in Fig. 8a, b and c respectively. In general, columnar beta grains were observed, with more equiaxed grains present as the power was increased and

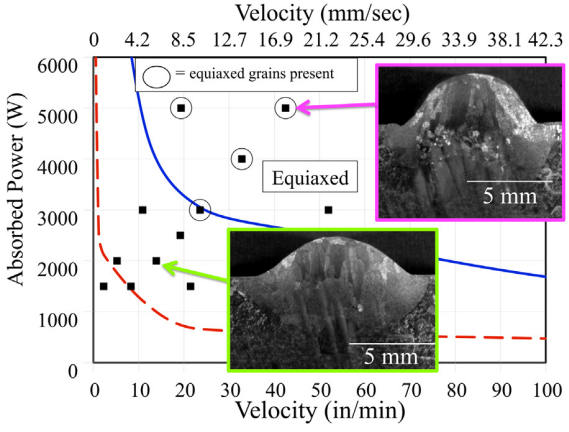

Fig. 7. Identification of melt pool cross sections with clear indications of equiaxed grains.

the area remains constant. It should be noted that the substate used in these experiments was a laminated Ti64 plate, yielding a layered appearance to the substrate in some of the micrographs.

Qualitative observations of Fig. 8 indicate that the beta grain size remains constant for power and velocity combinations with the same melt pool area. Furthermore, the micrographs for different melt pool areas, which are scaled to make the melt pool areas roughly the same size (though they differ over a factor of 4), also have beta grains that appear to be similarly sized. This suggests that the beta grain sizes are scaling with the sizes of the melt pool areas. The beta grain widths and melt pool areas have been quantitatively measured, and measurements have been averaged for the blue, red and green experimental cases. The measured effective melt pool width was calculated from the measured area assuming the area is a semi-circle and the width is the diameter of the circle. For the blue, red and green cases of constant area, the beta grain sizes are 321.8 ± 37.7 μm, 417.1 ± 28.1 μm and 538.2 ± 37.1 μm and the effective measured widths are 6193 ± 253 μm, 9496 ± 868 μm and $12{,}960 \pm 1103$ μm, respectivley. The average beta grain width was plotted against the average experimentally measured effective melt pool width in Fig. 9, with error bars showing the standard deviation of measured results. The data points tend to fall on a straight line, indicating a constant ratio of beta grain width to effective melt pool width. In all experimental cases, approximately 20 beta grains were seen across the melt pool width.

The results of this study are thus yielding substantial insight into the subject of beta grain size control for AM of Ti64. Control of melt pool cross sectional area also approximately controls solidification cooling rate. This in turn leads to control of beta grain size, namely beta grain width. This then ultimately leads to a simple scaling factor between melt pool width and beta grain size, so that as melt pool width is varied, beta grain size also changes to consistently yield approximately 20 grains across

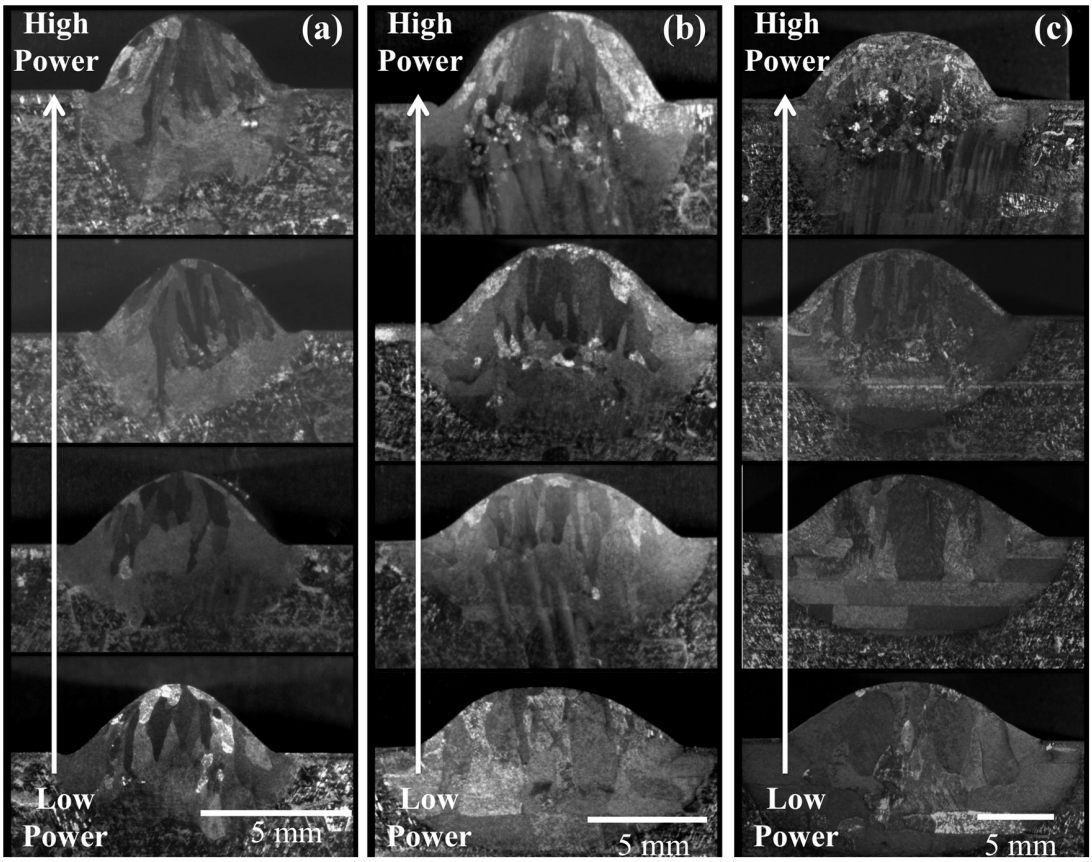

Fig. 8. Solidification microstructure for melt pool cross sectional areas (a) 0.016 in^2/10.3 mm^2, (b) 0.032 in^2/20.6 mm^2 and (c) 0.064 in^2/41.2 mm^2.

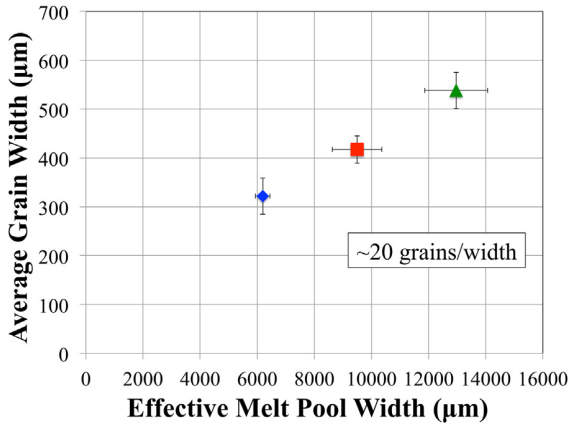

Fig. 9. Experimentally determined grain size scaling with melt pool width.

the melt pool width. This result is seen for a single bead geometry and this particular AM process. Investigations are underway regarding the robustness of this finding for different deposition geometries using wire feed e-beam AM and for other direct metal AM processes acting in different regions of processing space.

6. Conclusions

Part and process qualification is an important concern within the AM field. This paper gives related insight into regions of processing space that can produce desired solidification microstructures. A P-V (beam power and beam travel velocity) process map has been created for single bead deposition of Ti64, which predicts solidification microstructure in terms of process variables. Curves of constant beta grain size and regions of grain morphology were identified in beam power *versus* velocity space.

Comparing the microstructure process map to the process map for controlling melt pool dimensions exposes relationships that can potentially be used to indirectly control solidification microstructure through melt pool dimension control. Results demonstrate that a constant melt pool cross sectional area results in a constant grain size throughout processing space for the electron beam wire feed process. Similarly, monitoring the melt pool length to depth ratio can be used to control the grain morphology. Experimental results support the numerical predictions. Along a line of constant area, increased power results in an increase in the population of equiaxed grains with a constant grain size. Additionally, increasing the melt pool area increases the grain size, with the beta grain width roughly scaling by a ratio of 20 grains per melt pool width.

In situ microstructure control is possible by monitoring melt pool dimensions in real-time. By integrating solidification microstructure and melt pool dimension control, balancing of high deposition rates, fine features and tailored microstructures results in efficiently produced near net shape parts with a

consistent and predictable microstructure. This result can greatly accelerate process qualification and potentially allow for tailored microstructure and resulting mechanical properties for the desired application.

Acknowledgements

This research was supported by a National Defense Science and Engineering Graduate (NDSEG) Fellowship, and by the National Science Foundation under grant CMMI-1131579.

References

[1] Taminger KM, Hafley RA. Electron beam freeform fabrication for cost effective near-net shape manufacturing. In: NATO/RTOAVT-139 specialists meeting on cost effective manufacture via net shape processing. 2006.
[2] Grylls R. Laser engineered net shapes. Adv Mater Process 2003:45.
[3] Beuth J, Klingbeil N. The role of process variables in laser-based direct metal solid freeform fabrication. JOM 2001:36–9.
[4] Vasinonta A, Beuth J, Griffith M. Process maps for predicting residual stress and melt pool size in the laser-based fabrication of thin-walled structures. J Manuf Sci Eng 2007;129(1):101–9.
[5] Fox J, Beuth J. Process mapping of transient melt pool response in wire feed E-beam additive manufacturing of Ti-6Al-4V. In: Freeform fabrication proceedings. 2013. p. 675–83.
[6] Beuth J, Fox J, Gockel J, Montgomery C, Yang R, Qiao H, et al. Process mapping for qualification across multiple direct metal additive manufacturing processes. In: Solid freeform fabrication proceedings. 2013. p. 655–65.
[7] Arcella F, Froes F. Producing titanium aerospace components from powder using laser forming. JOM 2000;52:28–30.
[8] Eylon D, Newman JR, Thorne JK. Metals handbook, vol. 2, 10th ed. Materials Park, OH: ASM International; 1990.
[9] Donachie M. Titanium a technical guide. ASM; 2007.
[10] Lutjering G, Williams JC. Titanium. 2nd ed. Springer; 2007.
[11] Kobryn P, Semiatin S. Microstructure and texture evolution during solidification processing of Ti-6Al-4V. J Mater Process Technol 2003;13:330–9.
[12] Baufeld B, Van der Biest O, Gault R. Additive manufacturing of Ti-6Al-4V components by shaped metal deposition: microstructure and mechanical properties. Mater Des 2010;31:106–11.
[13] Murr LE, Esquivel EV, Quinones SA, Gaytan SM, Lopez MI, Martinez EY, et al. Microstructures and mechanical properties of electron beam-rapid manufactured Ti-6Al-4V biomedical prototypes compared to wrought Ti-6Al-4V. Mater Charact 2009;60:96–105.
[14] Brandl E, Leyens C, Palm F. Mechanical properties of additive manufactured Ti-6Al-4V using wire and powder based processes. Trends Aerosp Manuf 2009.
[15] Brandl E, Schoberth A, Leyens C. Morphology, microstructure, and hardness of titanium (Ti-6Al-4V) blocks deposited by wire-feed additive layer manufacturing (ALM). Mater Sci Eng A 2012;532:295–307.
[16] Antonysamy A, Prangnell P, Meyer J. Effect of wall thickeness transitions on texture and grain structure in additive layer manufacture (ALM) of Ti-6Al-4V. Mater Sci Forum 2012:205–10.
[17] Puebla K, Murr L, Gaytan S, Martinez E, Medina F, Wicker R. Effect of melt scan rate on microstructure and macrostructure for electron beam melting of Ti-6Al-4V. Mat Sci Appl 2012;3:259–64.
[18] Hrabe N, Quinn T. Effects of processing on microstructure and mechanical properties of a titanium alloy (Ti-6Al-4V) fabricated using electron beam melting (EBM), Part 1. Distance from build plate and part size. Mater Sci Eng A 2013;573:264–70.
[19] Hrabe N, Quinn T. Effects of processing on microstructure and mechanical properties of a titanium alloy (Ti-6Al-4V) fabricated using electron beam melting (EBM), Part 2. Energy input, orientation and location. Mater Sci Eng A 2013;573:271–7.
[20] Bontha S, Klingbeil N. Thermal process maps for controlling microstructure in laser-based solid freeform fabrication. In: Solid freeform fabrication proceedings. 2003. p. 219–26.
[21] Bontha S, Klingbeil N, Kobryn P, Fraser HL. Effects of Process Variables and Size Scale on Solidification Microstructure in Beam-Based Fabrication of Bulky 3D Structures. Mater Sci Eng A 2009;514:311–8.
[22] Bontha S, Klingbeil N, Kobryn P, Fraser H. Thermal process maps for predicting solidification microstructure in laser fabrication of thin wall structures. J Mater Process Technol 2006;178:135–42.
[23] Kobryn P, Moore E, Semiatin S. The effect of laser power and traverse speed on microstructure, porosity and build height in laser deposited Ti-6Al-4V. Scr Mater 2000;43:299–305.
[24] J. Beuth, N. Klingbeil, and J. Gockel, Process mapping of cooling rates and thermal gradient, PCT/US2013/055422, August 16, 2013.
[25] Gockel J, Beuth J. Understanding Ti-6Al-4V microstructure control in additive manufacturing via process maps. In: Solid freeform fabrication proceedings. 2013. p. 666–74.
[26] Soylemez E, Beuth J, Taminger K. Controlling melt pool dimensions over a wide range of material deposition rates in electron beam additive manufacturing. In: Solid freeform fabrication proceedings. 2010. p. 571–82.
[27] Fox J. Unpublished research. Carnegie Mellon University; 2014. Internal report.
[28] Hunt JD. Steady state columnar and equiaxed growth of dendrites and eutectic. Mater Sci Eng 1984;65:75–83.
[29] ASTM Standard E112-13. Standard test methods for determining average grain size. West Conshohocken, PA: ASTM International; 2013.